BoxyBot II, the fish robot

Fin Design, Programmation, Simulation and Testing

January 8, 2010

EPFL - Semester Project

Author: Benjamin Fankhauser

Supervisor: Alessandro Crespi, Mathieu Perez

Professor: Auke Jan Ijspeert

Contents

1 Introduction

The goal of this semester project was to design a more recent version of the fish robot BoxyBot developped at the BIRG using the same new modules as for the Salamander Robot, focussing in particular on the design of the fins in terms of speed and efficiency and the comparison to the results obtained in simulation.

The project included the programmation of the microcontroller by means of simple sine waves for a start and by means of a central pattern generator (CPG) in a following step. It also included the design of a simple controller using two external cameras in order to have the robot swim in a straight line.

The conception of a new fish robot is part of the EU-funded ANGELS programm. The robot will be used for exploring close interaction between perception and action and multi-agent perception and communication.

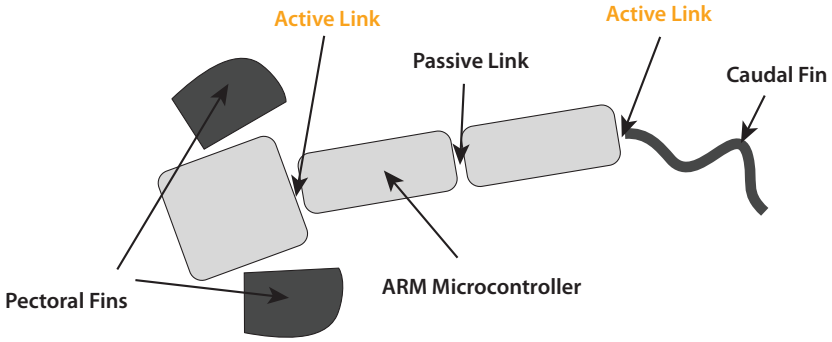

Figure 1: Active Caudal Fin Configuration

2 Methods and theory

This section deals with the theoretical aspects and methods, focussing first of all on the general design of the robot and on the fin design, including hypotheses on the relations between frequency, amplitude and speed, efficiency.

The following subsection then deals with the simulation of the behaviour of the robot, which parameters were used and how they could be obtained from the general design of the robot.

The final sections will then deal with the programmation of the microcontroller using sine waves and a CPG and the controlling of the robot using external sensor information.

2.1 General Design

The general design of the robot was mainly determined by the number of modules and their order. It was clear that there had to be a limb module which contained the articulations of the two pectoral fins and a motorized link to the next module. The number of body modules with only one motorized articulation was determined by the choice of the microcontroller.

The previous version of the BoxyBot fish robot used a PIC microcontroller [1]. The PIC had the advantage of a very small size which would allow us to implement it into the limb modulee. However, we decided to use an ARM Microcontroller for reasons of computational power. This would allow us to use a wirless radio connection developped at the BIRG between computer and robot. As the robot needs a connection to the computer for localisation, this proofed much more practical than establishing a physical link in addition as would have been necessary using a PIC microcontroller. Additionally this would have meant an influence on the results of the speed measures. Deciding for the ARM microcontroller on the other hand meant using an additional module that could not contain any motorized articulation due to the size of the microcontroller.

Furthermore, we decided using another module which would give the robot an additional degree of freedom. This allowed us not only to study the behaviour of the robot for a caudal fin articulated by two motorized modules, but proofed to be very effective for steering the robot.

These decisions allowed us to imagine three main configurations of the robot which are shown in figures 1 to 3. Interestingly the last configuration proofed to be very simple in controlling and the most stable in terms of swimming behaviour of the robot. In addition, it also presented the advantage of having an active caudal fin, so we finally decided to run our test with this configuration.

Please refer to the videos attached to this report for more information or have a look at the project's webpage at http://birg.epfl.ch/page71745.html.

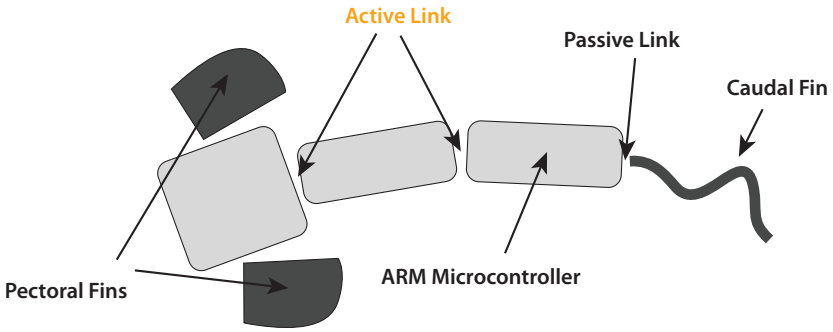

Figure 2: Passive Caudal Fin Configuration

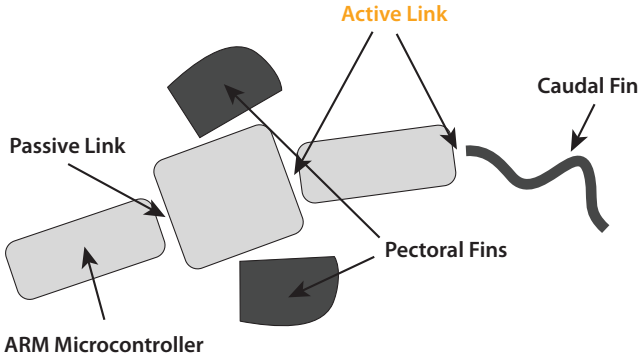

Figure 3: Head First Configuration

2.2 Fin Design

In the following we will present some methods of how to estimate the efficiency of the swimming behaviour of the robot and how it is influenced by the frequency and amplitude and the shape of the fins. The verficiation of these hypothesis figures in section 3.

2.2.1 Resonance Frequency

As could be shown in previous work [1], flexible fins can outperform rigid fins in terms of speed of the robot at a given speed. It could also be shown that for a rigid fin the speed of the robot increases linerarly with respect to the excitation frequency with which the caudal fin is articulated. For a flexible fin however there is something as a cut-off point at which the speed stops to increase for increasing frequencies.

We were convinced that this had something to do with the resonance frequency of the fin as the resonance frequency represents the frequency for which the amplitude of the fin (measured at the fin's trailing edge) is maximal. Thus increasing the frequency above the limit of the resonance frequency would not result in an increase, but rather a drop of the amplitude of the fin and therefore not in an increased speed.

Considering a fin with length l, width or height w and thickness t and using the approximation $t \ll w, l$, the resonance frequency of the fin is given by:

$$f_r = \frac{1}{2\pi} \cdot \sqrt{\frac{k}{m_f + m_a}} \tag{1}$$

where k is the spring constant, m_f the mass of the fin and m_a the so called 'added mass' which is due

to the fluid (water) surrounding the fin.

The spring constant is given by:

$$k = \frac{E \cdot I}{l^3} = \frac{E \cdot w \cdot t^3}{4 \cdot l^3} \tag{2}$$

where E is the young's modulus of the fin and I the cross sectional moment of inertia (CSMI) which is in our case given by:

$$I = \frac{w \cdot t^3}{12}$$

The mass of the fin is given by:

$$m_f = w \cdot l \cdot t \cdot \rho_f \tag{3}$$

where ρ_f is the density of the fin material.

The added mass according to [3], is given by:

$$m_a = \frac{\pi}{4} \cdot l \cdot w^2 \cdot \rho_w \tag{4}$$

where ρ_w is the density of water.

Using equations 2 to 4, 1 becomes:

$$f_r = \frac{1}{2\pi} \sqrt{\frac{E \cdot t^3}{(4 \cdot \rho_f \cdot t + \pi \cdot \rho_w \cdot w) \cdot l^4}} \tag{5}$$

We used artificial rubber as material for the flexible fins and therefore used $\rho_f = 1400 \, \frac{\text{kg}}{m^3}$. The density of water is given by $\rho_w = 1000 \, \frac{\text{kg}}{m^3}$ and, as the young's moduleus wasn't known, we determined it experimentally. It followed that for a given material and a rectangular type of fin the resonance freqency was determined by w, l and t .

Note that the resonance frequency of a fin in the air doesn't depend on the height w of the fin as we can neglect the term with ρ_w in comparison with the one of ρ_f. In water, however, this is not the case.

2.2.2 Efficiency Estimation

It is somewhat intuitive that the propulsion at the resonance frequency where the amplitude of the fin movement is maximal must be more efficient than at any other frequency. The speed however doesn't depend directly on the amplitude of the fin movement, but mainly on the thrust force due to a vortex field which is of course induced by the fin movement. Only knowing about the resonance frequency therefore does not necessarily include that the creation of the vortices is optimal.

In simulation we remedied at this problem by directly calculating the thrust force, which will be shown in the next section.

However there are some other fairly simple methods used to determine the efficiency of the movement of a caudal fin, as shown by [4][5].

The strouhal number gives us a simple measure of how good the creation of the vortices is and does not depend on a complicated and in practice almost impossible calculus as the thrust force calculation. Interestingly the strouhal number of most of the species using a fin or a flagellum for propulsion could be shown to be in the range of 0.25-0.4 and seems to be independent of the size of the animal. It is be given by:

$$St = \frac{A \cdot f}{v} \tag{6}$$

where A is the maximum amplitude measured at the trailing edge, f is the excitation frequency and v the speed of the robot.

The froude number gives a measure of the maneuverability of the robot and gives the ration between inertial and gravitational force in the flow. It is given by:

$$Fr = \frac{v}{\sqrt{g \cdot L}} \tag{7}$$

where v is the speed of the robot, g is the gravity constant and L is the total length of the robot.

Finally, the Reynolds number tells us whether we have a laminar or turbulent flow around the robot. It is given by:

$$Re = \frac{v \cdot L}{\nu} \tag{8}$$

where v is the speed, L is the total length and ν is the viscosity of water.

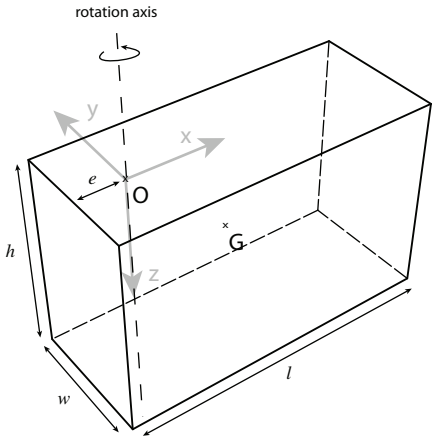

Figure 4: Schematic Description of the Robot's module

2.3 Simulation

For the simulation we used a simulator designed by Mathieu Perez from the BIRG. In the following we will focus on the parameters that are necessary to describe the robots behaviour and which are therefore indispensable to the simulation. As the robot can be seen as a chain of different modules and corresponding interconnections, we'll focus in the first part on the parameters that describe the modules and in the second part on the ones that define the module's interconnections.

Note that the simulator only calculates the behaviour of the robot on a horizontal plane and does not simulate its movement in the vertical direction. We could therefore only take measures with respect to the movement of the caudal fin and did not take into account any movement of the pectoral fins.

2.3.1 Description of the robot's modules S

To simplify the simulation process we used a rectangular block as a more or less accurate approximation of the robot's modules. It can be shown that any module can be sufficiently described by 15 parameters which we will briefly discuss in the following.

Among these parameters figure first of all the length l, the width w and the height h of the module (cf. figure 4). The parameter e can be understood as the difference between the beginning of the module and the rotation axis of the joint. And finally we have the weight m of the module.

The remaining parameters i.e. the first inertial vector $\vec{m_s}$ and the interial matrix $\widehat{I_o}$ describe the inertial properties of the module. The inertial vector is defined as follows:

$$\vec{m_s} = m \cdot \vec{OG}$$

where m is the mass of the module and $\vec{OG}$ is the distance of the module's center of gravity G to the origin O or rather the joint's rotation axis in our case. Now, as we suppose the center of gravity to coincide with the center of the module we may write the previous equation as follows:

$$\vec{m_s} = \begin{pmatrix} m_{s,x} \\ m_{s,y} \\ m_{s,z} \end{pmatrix} = m \cdot (\frac{l}{2} - e) \cdot \begin{pmatrix} 1 \\ 0 \\ 0 \end{pmatrix} \tag{9}$$

Note that we chose $m_{s,z} = 0$ because of our method of simulation.

The inertial matrix is a symetrical matrix defined with respect to the origin O and given by:

$$\widehat{I_o} = \begin{pmatrix} I_{O,xx} & I_{O,xy} & I_{O,xz} \\ I_{O,yx} & I_{O,yy} & I_{O,yz} \\ I_{O,zx} & I_{O,zy} & I_{O,zz} \end{pmatrix} \tag{10}$$

The elements of the matrix are given by:

$$I_{O,xx} = \frac{m}{12} \cdot \left(h^2 + w^2\right)$$

$$I_{O,xy} = 0$$

$$I_{O,xz} = 0$$

$$I_{O,yy} = \frac{m}{12} \cdot \left(l^2 + h^2\right) + m \cdot (\frac{l}{2} - e)^2$$

$$I_{O,yy} = 0$$

$$I_{O,zz} = \frac{m}{12} \cdot \left(l^2 + w^2\right) + m \cdot (\frac{l}{2} - e)^2$$

Note that in our case the matrix is actually diagonal. For a more detailed explanation consult the appendice.

2.3.2 Description of the interconnections L

Overall there are three different types of interconnections, motorized or elastic interconnections and a head interconnection.

The head interconnection of type t is no real interconnection but figures here mainly to match the number of segments. It only takes the parameter d which represents the distance between the origin O of the first module and that of the second module which equals the distance l of the module in our case. Note that the first interconnection is always one of type t and that there is only one such connection.

The motorized interconnections of type m can each be described by ten parameters. The already mentionned distance d, a certain factor p which defines whether the motorized link is rigid (p=0) or elastic (p=1, never used in our case), the inertia of the motor J_m before reduction and the reduction ratio N which defines the total motor inertia $I_m = J_m \cdot N^2$. Then there is the offset ϕ, the amplitude A and the frequency ν which will give the output behaviour in form of a sine wave $Q = A \cdot \sin(2\pi \cdot \nu t - \phi)$ for every motorized link and finally there are the three parameters K_p,T_i and T_d of the PID controller of the motor.

The elastic interconnections of type e are especially useful for simulating a flexible fin. They are described by parameter d, and the stiffness r of the link. In order to simulate our flexible caudal fin we represented it as a succesion of a number n of smaller rigid segments with elastic interconnections and a stiffness that was given by $r = \frac{E \cdot I}{dx}$, where E is the young's modulus, I the cross sectional moment of inertia and dx the length of each small segment, given by $dx = \frac{l}{n}$, where l is the length of the caudal fin.

2.3.3 The Simulator

The simulator itself takes two input files, one that describes the robots modules and interconnection we discussed previously and one that specifies some general parameters like the hydromechanic parameters, the initial position of the robot, the simulation time, the duration of each timestep etc. For more detailed information one might want to refer to the files robot.dat and config.dat that figure among the example files attached to this report and which show the configuration for a robot with one limb and two body modules as well as a segment which represents the fixation of the caudal fin and a 18 small segments which represent a flexible caudal fin.

The simulator produces an output file with the following values at each timestep t. The speed vector $\vec{v} = (v_x, v_y, v_z)^T$, the orientation of the head given by the roll angle θ_x, the pitch θ_y and the yaw θ_z of which only the yaw is used in our case (the others are always zero), the position of the head is given by the position vector $\vec{x} = (x, y, z)^T$ and a description of the robot's position and orientation using quaternion notation, thus $\{\lambda_0, \lambda_x, \lambda_y, \lambda_z\}$. It then gives the speed of every motorized and elastic link $\omega_i = \frac{d\phi_i}{dt}$ as well as the angle ϕ_i for every interconnection which corresponds to the angle between the current and the initial position. One might refer to the example files attached to this report.

We used matlab in order to facilitate and automatize the simulation input and to represent the obtained data in either graphs or videos. Example files are equally attached. Note that we made good use of the configuration function 'HeadFixed' in the 'config.dat' file in order to determine whether we would fix the robot's head in order to extract some caudal fin characteristics or whether we would let it move freely in order to simulate the real robots behaviour.

2.4 Programmation

2.4.1 Sine Wave Functions

The programmation of the robot was first done by simply using a sine function for every interconnection specified by the amplitude A_i, the frequency ν_i and the offset ϕ_i as follows:

$$\theta_i = A_i \cdot \sin(2\pi \cdot \nu_i \cdot t + \phi_i) \tag{11}$$

where θ_i is the set-point of each interconnection (in radians).

The value of every θ_i was calculated at every timestep, using not a fixed timestep but calculating as fast as the microcontroller would allow. The value would then be sent to the motors which would adjust their position. The amplitude, ferquency and offset of every interconnection could be changed online using the a wirless radio tool developped at BIRG. We used an sine lookup table with 800 values for computational reasons.

Please refer to the example files attached to the report. The corresponding code figures in the file 'mode.c'.

2.4.2 Central Pattern Generator

One of the drawbacks of the method used in the previous section is that the depending on the position of the motors a change of parameters could result in very abrupt changes on the position of the motors which would cause unwanted disturbances in the water and could even harm mechanical parts. We therefore used a central pattern generator (CPG) which allowed smoother changes in position, as could be shown by work on the previous version of the robot [6].

We implemented a system of four coupled amplitude-controlled phase oscillators, one per fin and one for the additional body segment (cf. figure 5). Each oscillator i was implemented as follows:

$$\dot{\phi_i} = \omega_i + \sum_j (\omega_{ij} \cdot r_j \cdot \sin(\phi_j - \phi_i - \varphi_{ij})) \tag{12}$$

$$\ddot{r_i} = a_r \left(\frac{a_r}{4}(R_i - r_i) - \dot{r_i} \right) \tag{13}$$

$$\ddot{x_i} = a_x \left(\frac{a_x}{4}(X_i - x_i) - \dot{x_i} \right) \tag{14}$$

$$\theta_i = x_i + \cos(\phi_i) \tag{15}$$

where θ_i is the set-point for each motor (in radians) and ϕ_i, r_i and x_i are internal state variables corresponding to the current phase, amplitude and offset of the oscillators. The control parameters are the desired frequency ω_i, the desired amplitude R_i and the desired offset X_i. ω_{ij} are the coupling weights and determine how much oscillator i is influenced by oscillator j. They are set to 0.5 omitting self-coupling i.e. $\omega_{ii} = 0 \; \forall i$. φ_{ij} are phase biases which are all set to zero in our case. The parameters a_r and a_x are constant positive gains set to 20 rad/s in our case. The zero offset for the pectoral fins is when they are turned backwards in a horizontal position, for the body segement and the caudal fin a zero offset is when they are in the sagittal plane.

The CPG asymptotically converges to a limit cycle where the phase difference between all four oscillators will be $\Delta\phi_{ij} = 0$ from almost any initial conditions [7] and the set-point becomes:

$$\lim_{t \to \infty} \theta_i(t) = X_i + R_i \cdot \cos(\omega_i t + \phi_{0,i}) \tag{16}$$

Figure 6 shows the convergence of the oscillators of the four interconnections from randomly chosen initial conditions to a general ryhtmic behaviour. The output angle (in °) corresponds to the actuator set-point (in radians). Note that the caudal fin and the body segment have the same amplitude, but have a phase difference of π. The pecotral fins are in phase with the caudal fin but have a smaller amplitude and a general negative offset which would make the robot go to the surface in a real world environment.

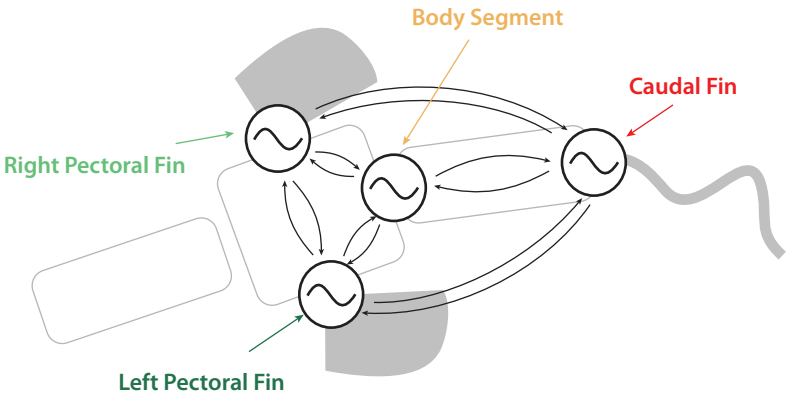

Figure 5: CPG control structure using four coupled amplitude-controlled phase oscillators

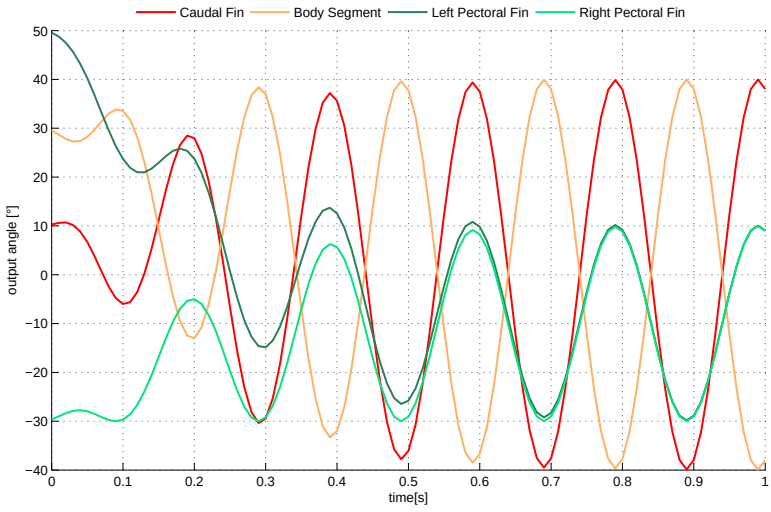

Figure 6: Convergance of the oscillators to a rhythmic output pattern with different desired output angles, amplitudes and offsets for the robot

2.5 Control

The position of the head of the robot could be determined using two external cameras and a corresponding code had been implemented by Alessandro Crespi and Matthieu Perez from the BIRG thus allowing to detect several LEDs moving around in the pool. Unfortunately we only had the opportunity to use a very simple control which would allow us to do the speed measures.

To detect the absolute position and orientation of the robot it would have been necessary to detect three points of the robot. Instead, we used only one LED as a reference point, the one of the head module and used always the same initial position for the robot in order to make sure that the orientation was known. We then set up a proportional controller that acted on the position error in the y-direction which corresponded to the width of the pool and made the robot swim along a straight line in the middle of the pool. It changed the desired offset of the caudal fin X_0 and the body segment X_1as follows:

$$X_0 = K_{p0} \cdot e \tag{17}$$

$$X_1 = K_{p1} \cdot e \tag{18}$$

where $e = (pos_y - 0.7)$ is the error between the actual and the desired position (in meters) and K_{po} and K_{p1} are the proportional gain in a range of 150-400 depending on the frequency and speed of the robot.

3 Measures and Results

This section deals with the measures of amplitude of the caudal fin and corresponding speed of the robot with respect to the resonance theory frequency as well as efficiency estimation methods established in the previous section. We will also compare these results to the ones obtained by simulation.

As the young's modulus E of the caudal fin material was not known we had to determine it first, in order to make reliable predictions on the maximum amplitude and speed of the robot.

3.1 Determination of the young's modulus

For the determination of the young's modulus we had to detect the maximum amplitude for a given fin. We therefore had to establish a full frequency plot in the range of 0.5-4.0 Hz. With a rough approximation we made sure that the resonance frequency would actually lie in this range. As the size of the fin with $l = 0.06$ m and $w = 0.04$ m and $t = 0.003$ m was rather small and on top of that it was also flexible we could make sure that the motor articulating the caudal fin was actually able to do an excitation of 40° up to a frequency of 4 Hz. This had also been shown by previous work [1].

For measuring we used a Canon PowerShot SX100 IS Camera with a video resolution of 640x480 pixels and 25 pictures per second. This was fairly enough, because the movement of the fin was sinusoidal which means that at the extremities, which we wanted to measure, the fin came to an almost complete standstill and the motion blur was very small. Alas, we could not use the fix installed cameras of the pool as their field of view was ways to large to measure any changes in the amplitude. To make use of the preinstalled tracking system we would also have had to put a LED on the trailing edge of the caudal fin, which could have influenced the result of the tests.

To determine the amplitude we used a transparent sheet of A4 paper with a grid which allowed us to have an accuracy of about 1 mm. The robot was immersed in the pool and, as good as possible, fixed to the ground. The camera was fixed on a tripod and with a frequency step of 0.1 Hz video sequences of 15 seconds duration were taken and the amplitudes determined. Because the process of determining the amplitude was very time consuming we took one value over all the range, and five in the zones of interest, i.e. the zone around the suspected resonance frequency.

Figure 7 shows the result of the measures. We can clearly observe that there is a maximum amplitude, although the low quality factor of the resonance curve makes it hard to determine it very precisely. We found the highest mean of fin amplitudes at $A_{max} = 77 \pm 1$ mm for a frequency of $f_r = 1.8 \pm 0.1$. Using this value and equation 5, the young's modulus can be computed easily and is $E = 9 \pm 1$ MPa. Please refer to the appendice for a detailed calculus.

Note that the amplitude of the flexible fin is bigger than the one of a rigid fin over a spectrum of over 2 Hz. This might be the reason why it could be shown previously [1] that for some frequencies flexible fins outperform rigid ones in terms of speed of the robot.

Once the young's modulus was determined, we could then predict the resonance frequency of fins of different size.

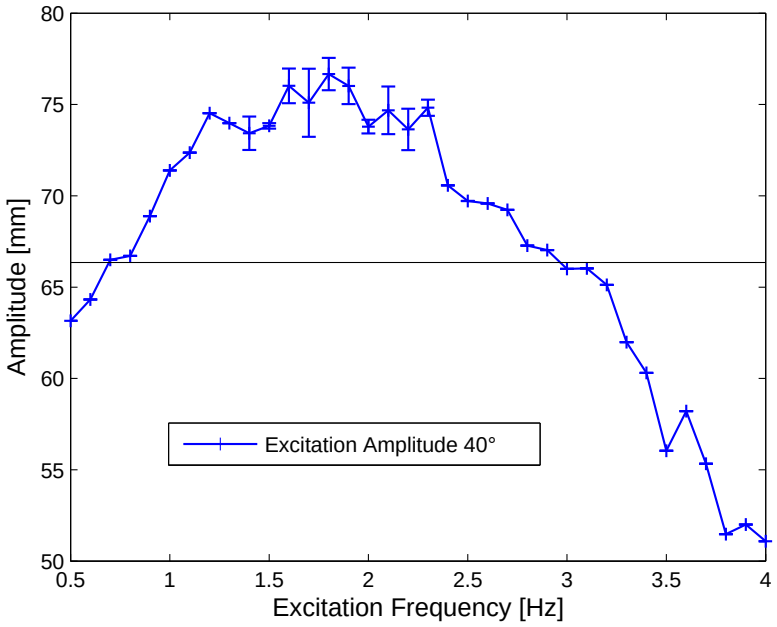

Figure 7: Amplitude vs. frequency for a caudal fin of 60x40 mm, the black line indicates the amplitude of a rigid fin of same size, the error bars show the standard deviation

3.2 Maximum Caudal Fin Amplitude

In a next step we wanted to look at the influence of the height w of the fin and the excitation amplitude on the amplitude of the fin and it's resonance frequency. Furthermore, we also wanted to compare these measures with results from the simulation.

3.2.1 Measured Resonance Curve

We proceeded in much the same way as explained in the previous section, using two different caudal fins. Fin 1 with $l = 0.095$ m, $w = 0.04$ m and $t = 0.003$ m has a resonance frequency at $f_{1R} = 0.7 \pm 0.1$ Hz. Fin 2 with $l = 0.095$ m, $w = 0.06$ m and $t = 0.003$ m has a resonance frequency at $f_{2R} = 0.6 \pm 0.1$ Hz. This is somewhat intuitiv, for as the bigger the fin is, the more it must feel the resistance of the water which tends to decrease its amplitude. Thus, for a bigger fin the point at which we have a maximum amplitude i.e. resonance must be at a lower frequency than for a smaller fin.

We chose the size of the fins so as to have a quite low resonance requency which would make measures simpler and avoid that too fast a movement would add some noise. Again, we could make sure that the motor was actually able to do a full 80° excitation amplitude up to a frequency of 1.6 Hz. Note that the length of the fin is equal to the length of the body and limb modules. Fin 2 has also the same height as the modules.

Figure 8 and 9 show the results for the two fins and table 1 gives an overview on the value of the maximum amplitude and resonance frequency. Note that the error bars mark the standard deviation.

We have to admit, that none of the maximum amplitudes are significantly different from the ones of their neighbouring frequencies. However we can see that our theoretical values are confirmed. Note that it seems as though the resonance frequency, and all the resonance curve with it, is shifted to the left for higher excitation amplitudes. This makes sense as the resistive force of the water must be higher because we accelerate the fin faster and up to a higher speed. Note also that the difference between a flexible and a rigid fin seems to be smaller for higher excitation amplitude, for an excitation

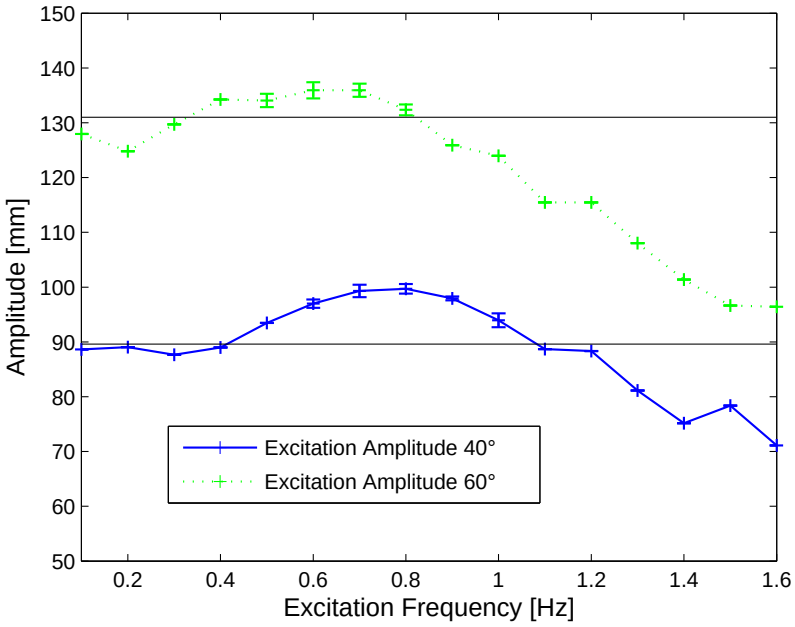

Figure 8: Amplitude vs. frequency for a caudal fin of 95x40 mm with $f_{1R} = 0.7 \pm 0.1$ Hz, the black lines indicate the amplitude of a rigid fin of same size

Fin	Theoretical f_r [Hz]	Excitation Amplitude [°]	Maximum Fin Amplitude [mm]	Measured f_r [Hz]
1	0.7 ± 0.1	40	100 ± 1	0.8
1	0.7 ± 0.1	60	136 ± 1	0.7
2	0.6 ± 0.1	40	99 ± 1	0.7
2	0.6 ± 0.1	60	136 ± 1	0.5
2	0.6 ± 0.1	80	167 ± 2	0.5

Table 1: Overview of the measured maximum fin amplitude and resonance frequency of the two fins for different excitation amplitudes

amplitude of 80° it even seems to be lower than for an rigid fin. This is certainly due to the same effect.

Note that the unexpectedly high values for an excitation amplitude of 80° in the range of 0.8-1.1 Hz were due to the creation of very strong vortex fields which would heavily influence the amplitude of the fin. For the rest of the measures and especially for the zones of interest we made sure that such effects did not occur and that the flow around the fin was not all that turbulent. To see some videos of this effect, please refer to the homepage of this project at http://birg.epfl.ch/page71745.html or to the files attached to this report.

Figure 10 shows a comparison plot of the two fins for 40° and 60° excitation amplitude. As we can see the bigger fin has in general a smaller amplitude. This is quite intuitive, as the fin meets more water per area and the inertial force must therefore be bigger. However, we can see that the value of the maximum amplitude doesn't change for a different height w of the fin (cf. table 1), which is quite astonishing. We might argue that the transfer from potential energy (battery) to mechanical energy must be so optimal that it doesn't depend on the size of the fin, but is rather limited by other physical constraints as the value of E for example.

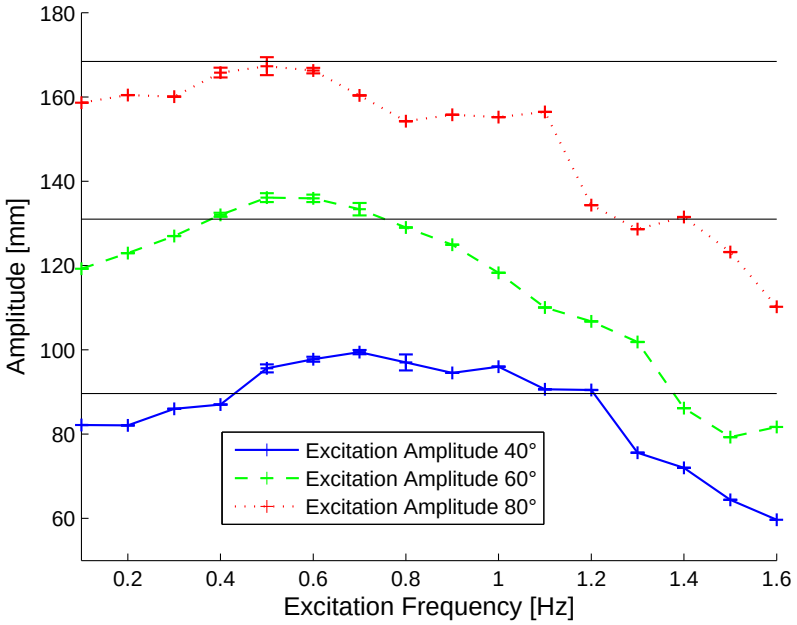

Figure 9: Amplitude vs. frequency for a caudal fin of 95x60 mm with $f_{2R} = 0.6 \pm 0.1$ Hz, the black lines indicate the amplitude of a rigid fin of same size

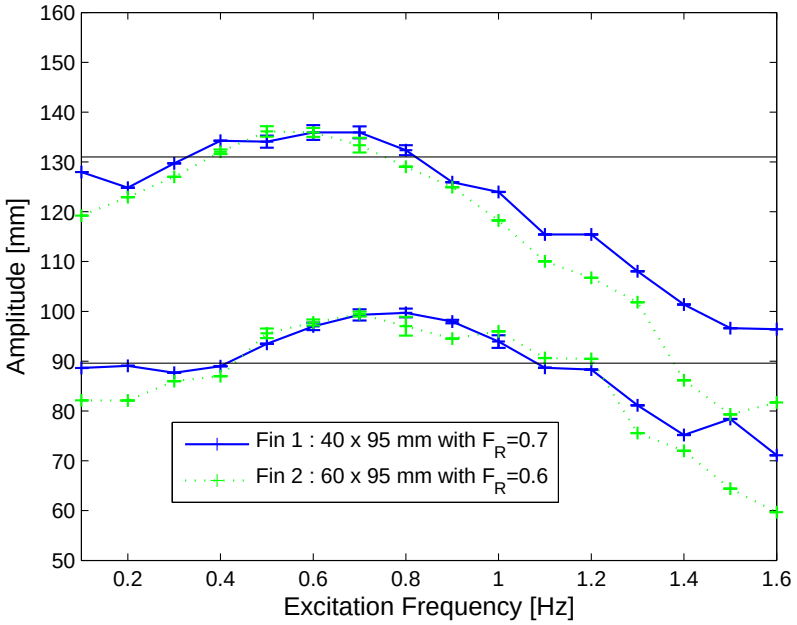

Figure 10: Amplitude vs. frequency for fin 1 and 2 at respectively 40° and 60° excitation amplitude, the black lines indicate the amplitude of a rigid fin of same size

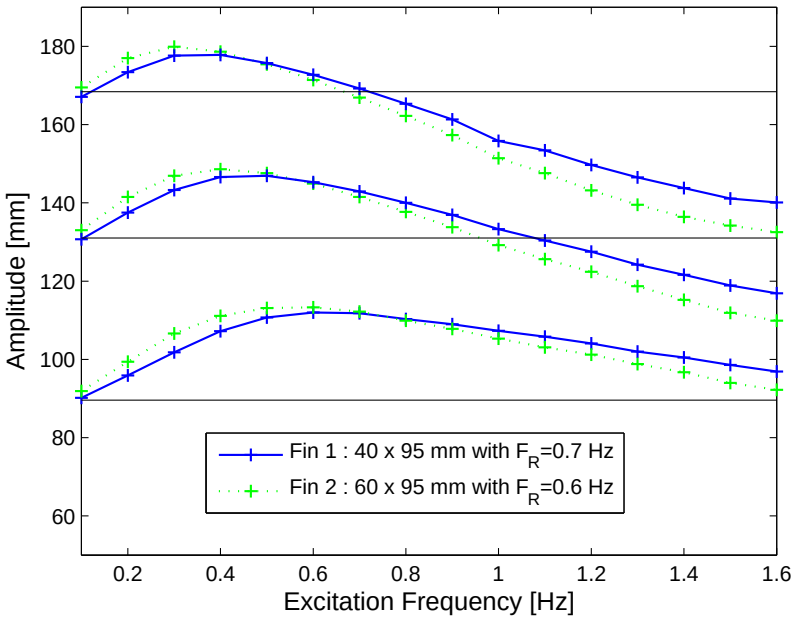

Figure 11: Simulated amplitude vs. frequency for the two fins at respectively 40°, 60° and 80° excitation amplitude, the black lines indicate the amplitude of a rigid fin of same size

3.2.2 Simulated Resonance Curve

Using the simulator described in section 2.3 we were able to determine the simulated resonance curve, proceeding in a way similar to the one of the previous section. Note that we adapted some hydromechanic coefficients in the configuration file in order to get a more comparable amplitude. More sophisticated adaptation of these parameters would probably have allowed to have the results even closer to reality. Please refer to the appendice or the files attached to this report for more detailed information.

Figure 11 shows the results for the two fins and table 2 gives an overview on the maximum fin amplitude and resonance frequency.

We can again see that the amplitude for flexible fins is bigger than for rigid ones over a large spectrum of frequencies. We can also see that the resonance frequency is smaller for higher excitation amplitudes which is quite intuitive and corresponds to the findings in the real world. Thus limiting ourselves the resonance frequencies for 40° excitation amplitude and comparing its values with the theoretical ones we can see that it fits the expected value well.

We can also observe that the resonance curve for the bigger fin is shifted more to the left as expected due to the smaller resonance frequency. The quality factor for the bigger fin is higher i.e. the values of the amplitude of the resonance curve are more accentuated. A quick look at table 2 tells us that the values for the maximum amplitude are slightly higher for the bigger fin, which is what we expect, although in reality the difference is hard to tell.

Note that the difference between the amplitude at the resonance frequency and the ones of its neighbouring frequencies is very small. Already here we might guess that this might have a large impact on the speed in so far as the speed might still continue to increase considerably even above the limit of the resonance frequency (cf. section 3.2.4).

Fin	Theoretical f_r [Hz]	Ex. Amplitude [°]	Max. Fin Amplitude [mm]	Simulated f_r [Hz]
1	0.7 ± 0.1	40	112	0.6
1	0.7 ± 0.1	60	147	0.5
1	0.7 ± 0.1	80	178	0.4
2	0.6 ± 0.1	40	113	0.6
2	0.6 ± 0.1	60	149	0.4
2	0.6 ± 0.1	80	180	0.3

Table 2: Overview of the measured maximum fin amplitude and resonance frequency of the two fins for different excitation amplitudes

3.2.3 Simulation and Reality

Figure 12 shows the comparison of the resonance curves obtained in simulation with the ones obtained by measuring.

We can see that, although we have already adapted some coefficients in the simulator, the amplitudes are still quite high. Either this values still are not high enough or there are some additional turbulences created in the water and which the simulator does not take into account. Table 1 and 2 show that the maximal difference for the amplitude at the resonance frequencies is around 13 mm for 40° excitation amplitude, which is about 10%. It is clear, though, that the difference between a flexible and a rigid fin in terms of amplitude at the resonance frequency does get smaller for higher excitation amplitudes in simulation as well as in reality, as one might expect.

We can ovserve that the simulated resonance curves are slightly shifted to the left with respect to the measured ones. Again, this might be due to some bad adjustement of the hydromechanical parameters or some additional turbulences. This might also be one of the reasons why the actual values of the resonance frequencies correspond better to the expected ones than in simulation.

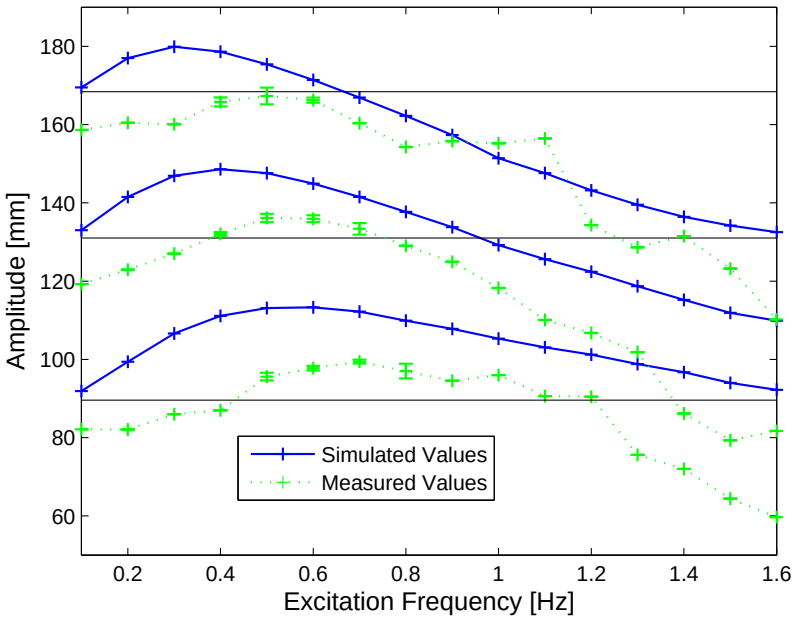

Figure 12: Comparison of amplitude vs. frequency for a caudal fin of 95x60 mm with $f_r = 0.6 \pm 1$ Hz at respectively 40°, 60° and 80° excitation amplitude in simulation and reality, the black lines indicate the amplitude of a rigid fin of same size

3.2.4 Simulating the Thrust Force

As metionned in section 2.2.2 the speed of the robot cannot be determined by the resonance frequency only, as the maximum of fin amplitude doesn't necessarily induce the stronges vortex fields. Knowing the speed of the motors and their angular positions, however, we were able to calculate the forward thrust force for every frequency (cf. appendice for detailed calculus). This allowed us to look for a link between resonance frequency and maximal speed.

Figure 13 shows a graph of the results for the two fins at respectivels 40° and 60° excitation amplitude.

Unfortunately we cannot observe any influence of the resonance frequency on the thrust force. This might be due to some badly adjusted parameters in the configuration file or due to this specific modelling. Note also that the actual speed is strongly influenced by the water resistivity and it could be that this graph is not so meaningful as we thought it to be.

We can see however that the thrust force is bigger for the second fin, even though the amplitude of the bigger fin is smaller for higher frequencies (cf. figure 10 and 11). This might explain why the fish is faster if propulsed by a bigger fin in a real world environement.

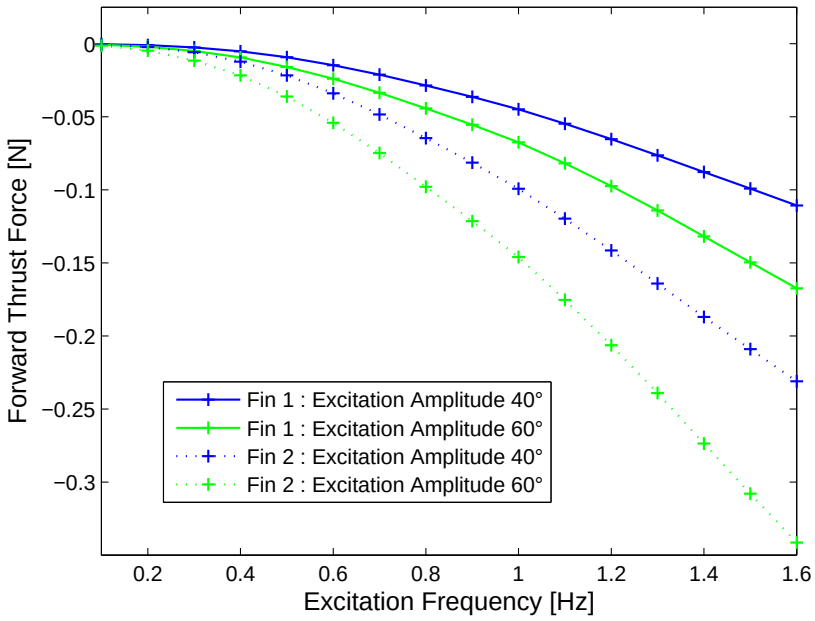

Figure 13: Simulated thrust vs. frequency for the two fins at 40° and 60° excitation amplitude

3.3 Speed Measures

This section deals with the speed of the robot due to a propulsion by using one of the two caudal fins mentionned in the previous section. We first of all verfied the correct behaviour of the robot due to the controller. We then looked at the influence of resonance frequency, the excitation amplitude, the size of the fin and did some measures for propulsion using more than just the caudal fin. Finally, we compared the obtained values to the ones obtained in simulation.

The speed measures were taken in a 1.2 x 6.0 x 0.3 m pool at the BIRG. Due to a precise balancing the robot would always swim at the surface of the water and using one of its fins for propulsion.

As mentionned in section 2.5 the measures were taken using two external cameras which would detect the LED integrated in the head module of the robot and determine its position (in meters) according to a reference frame fixed at one of the pool's corners. The position would be updated every 100 ms and stored in a tracking file which we used as a basis for the speed calculation. The position of the robot would also be used as an input signal to the controller of the robot as explained in section 2.5.

Five measures for the speed of the robot were taken for every frequency and amplitude. Each measure itself represented the average speed of the robot over a period of 5 seconds of swimming on a straight line using the controller. As the robot, due to the propulsion method, was doing quite an osciallatory movement we could not simply take the position at the beginning and at the end to calculate the speed, but we would calculate the speed for every timestep with respect to the position at the previous timestep and then take the average of these 50 speed measures. We took five measures of 5 seconds because we wanted to observe the speed at different locations in the pool and make sure that errors due to the correction of the swimming direction, which might have been rather abrupt at certain points, didn't influence the results in a negative way. Finally we made sure that no measurement was taken before the robot has been swimming for at least five seconds, for low frequencies we allowed up to 20 seconds. This would guarantee that the robot was not accelerating while we were taking the measures.

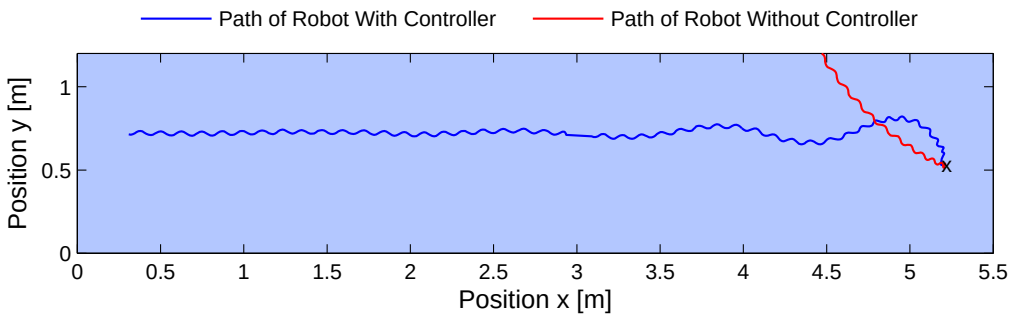

Figure 14: Movement of the Robot in the Pool starting at 'x' and moving to the left

Note that the errorbars on all the graphs depict the standard deviation.

We could see that the CPG command of the robot worked very well, was reliable and allowed smooth transitions for changes in amplitude, frequency and offset.

Please refer to the videos attached to this project to make yourself a general idea of the behaviour of the robot and its environement.

3.3.1 Controlling Robot Swimming

Figure 14 shows the path of a robot propelled by a caudal fin of 40 x 95 mm at $f = 1.0$ Hz and with an excitation amplitude of 60°.

We can observe that the robot bumps directly into a wall without the controller. Using the controller, the robot manages to follow a straight line in the middle of the pool.

Note that it becomes more difficult to control the robot at higher frequencies. This might be due to the fact that the robot moves faster, but also that, as it moves faster, the whole movement becomes more instable.

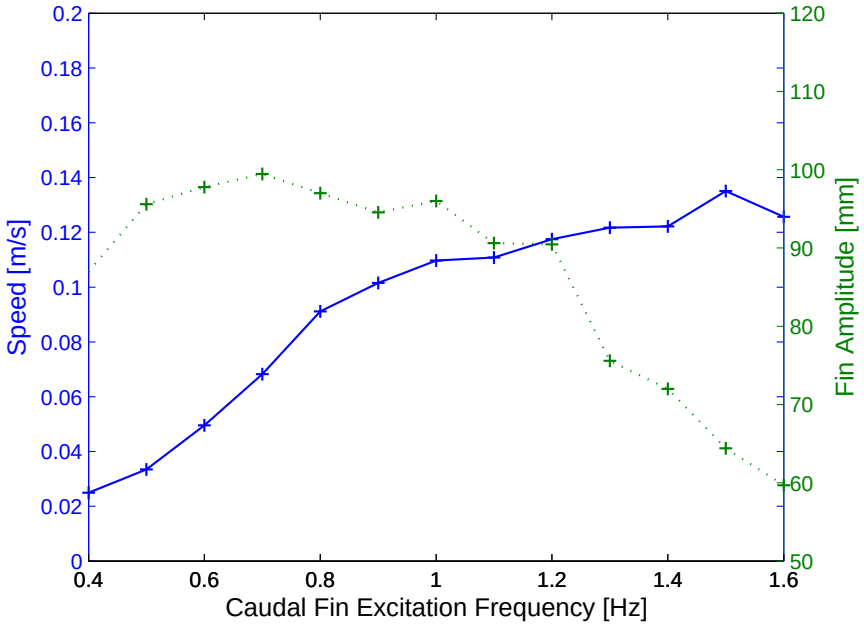

Figure 15: Amplitude and speed vs. frequency for a caudal fin of 95x60 mm with $f_{2R} = 0.6 \pm 1$ Hz at an excitation amplitude of 40°

3.3.2 Influence of the Resonance Frequency

Figure 15 shows the mean values of amplitude and speed versus the frequency of fin 2 for an excitation amplitude of 40°.

We can clearly see that the speed increases linearly with the frequency up to the limit of the resonance frequency and then almost stops increasing. It can be seen that the more the amplitude drops, the more the speed stops increasing. We might argue that the increase of frequency compensates for the drop in fin amplitude.

The somewhat retarded stopping of the speed increase with respect to the resonance frequency is probably due to the fact that the fin amplitude is still pretty close to the maximum fin amplitude (as mentionned in 3.2.2) even for frequencies above the limit of resonance frequency.

Nevertheless, we can say that the speed increase strongly depends on the resonance frequency.

Figure 16 shows the same graph for fin 1 and an excitation amplitude of 60°.

We can see that the same oveservations can be made, which further verifies our hypothesisses.

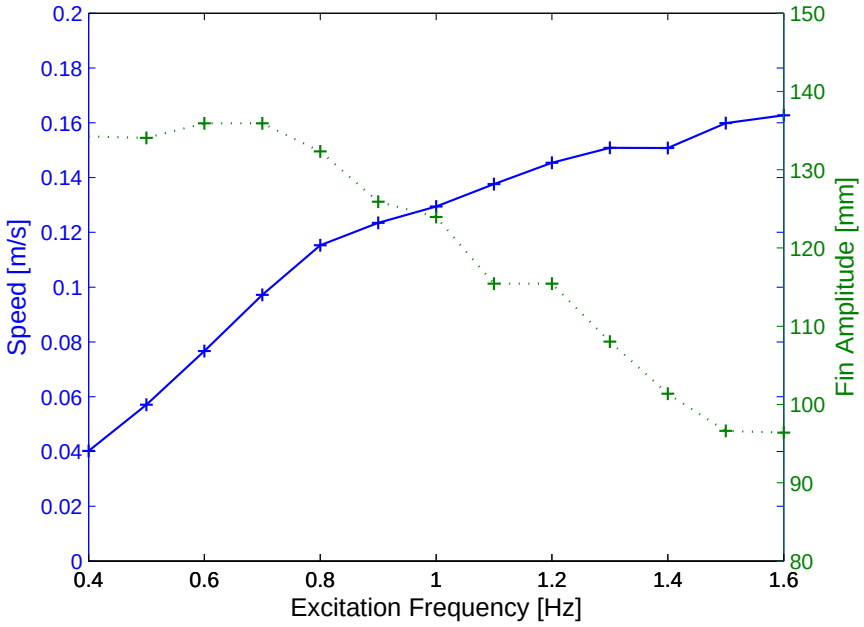

Figure 16: Amplitude and speed vs. frequency for a caudal fin of 95x40 mm with $f_{1R} = 0.7 \pm 1$ Hz at an excitation amplitude of 60°

3.3.3 Influence of the Excitation Amplitude

Figure 17 shows the influence of the excitation amplitude on the speed of the robot.

As expected, we can see that the faster the robot swims the higher the excitation amplitude is. This confirms expermintal findings for the previous version of the robot [1].

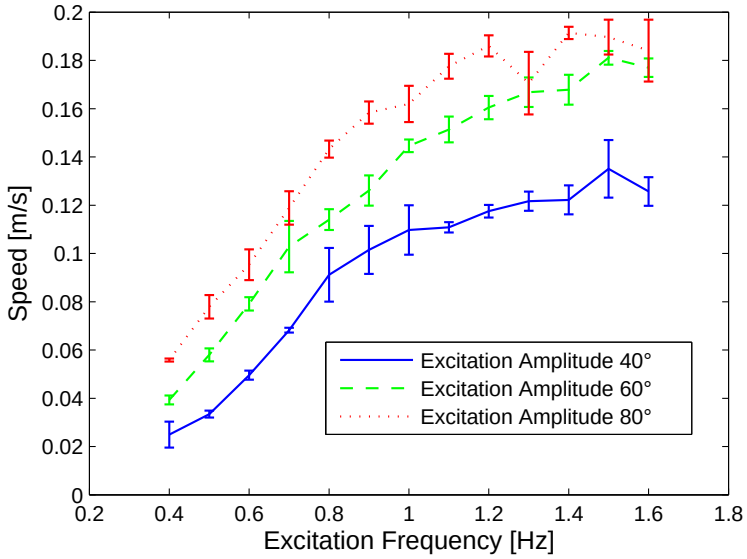

Figure 17: Speed vs. frequency for a caudal fin of 95x60 mm with $f_{2R} = 0.6 \pm 1$

3.3.4 Influence of the size of the fin

Figure 18 shows the result for fin 1 and fin 2 for an excitation amplitude of 60°.

As far as the lower frequencies are concerned, the difference in size of the fins does not have any influence of the speed. For higher frequencies, though, the bigger fin is faster, although the amplitude is smaller (cf. figure 10 and 11). However, this corresponds to the findings for the thrust force in simulation (cf. section 3.2.4).

Note that we cannot observe any difference in speed due to the difference in resonance frequency. This is certainly due to the low quality of the resonance curves and implies, as mentionned in section 3.3.2, that we must see the resonance frequency more as a broad phenomena that influences speed over a certain range of frequencies.

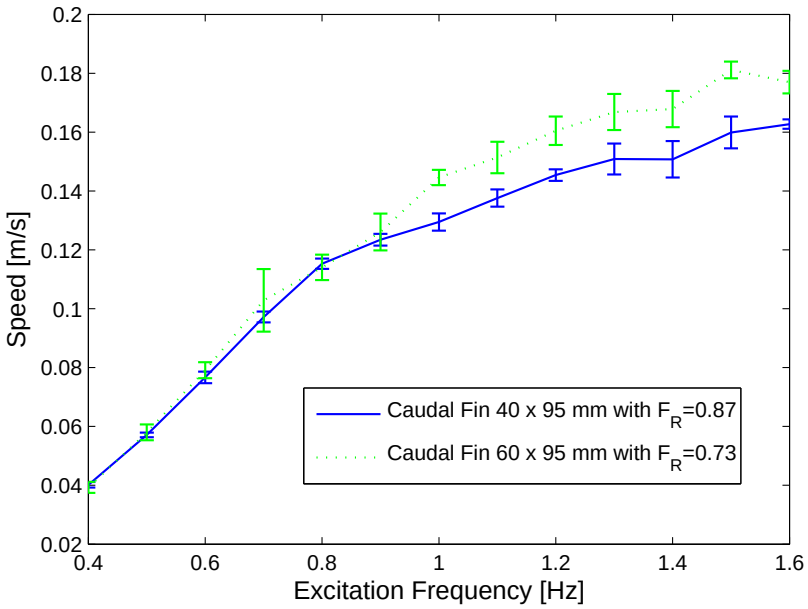

Figure 18: Speed vs. frequency for two different caudal fins for an excitation amplitude of 60°

3.3.5 Using the Body Segment

So far we had only considered propulsion by articulation of the caudal fin. We then wanted to focus on the effect of several articulations moving at the same time. First of all we wanted to use the body segment.

Figure 19 shows the results for caudal fin 2 with 80° excitation amplitude compared to the results for caudal fin 2 and the motorized body segment with 40° excitation amplitude each.

As we can see the use of the body segment results in a higher speed than using the double of the excitation amplitude of the caudal fin. This makes sense, as the part of the robot that is moving is longer in that case and therefore the amplitude must be higher.

Note that the speed tends to stop increasing around the resonance frequency in both cases which is a further proof of our hypothesis this concerning.

So far the offset $\phi_{0,i}$ between the two articulations as it figures in equation 16 was 0. In a next step we measured the speed for several different offsets. Note that in general the offset can be expressed as:

$$\phi_{0,i} = \frac{2\pi \cdot K \cdot i}{N} \tag{19}$$

where N is the total number of articulations, i is an integer that depicts the current articulation and K is a constant that defines the value of the offset.

As we have only 2 articulations in our case, we can write:

$$\phi_{0,0} = 0$$

$$\phi_{0,1} = K \cdot \pi$$

One can see that as the offset is part of a cosine (cf. equation 16), thus K is only meaningful in a range of [0,2], but as the cosine is an odd function around 1 in the range of [0,2], we can further reduce the range of K to [0,1].

Figure 20 shows the speed measures for different values of K and thus ϕ. We can see that a zero offset results in the highest speed. This means that the robot is faster in carangiiform than in

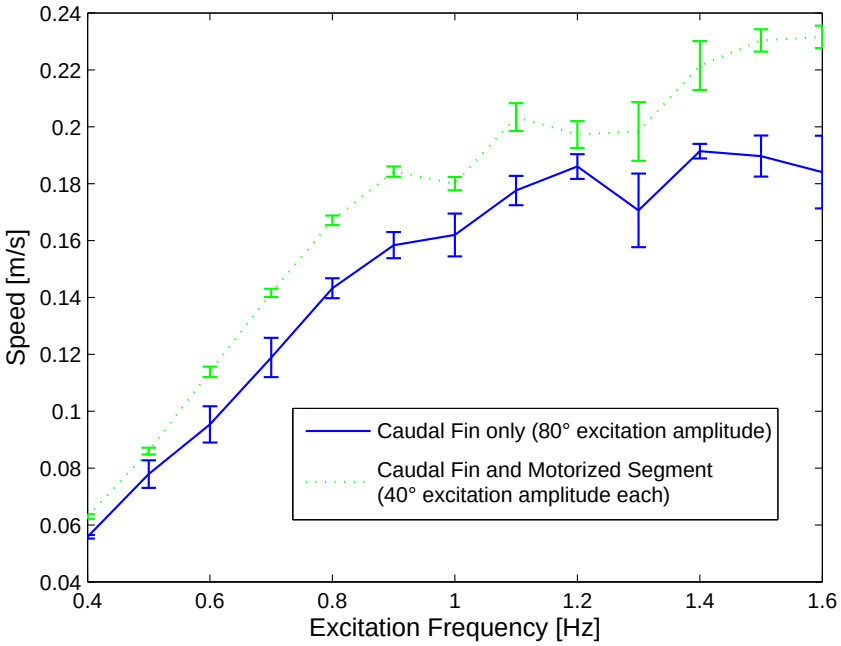

Figure 19: Speed vs. frequency for a caudal fin of 95x60 mm (and the motorized body segment)

anguiliiform propulsion, which is certainly due to its physical conception as for example the low number of articulations.

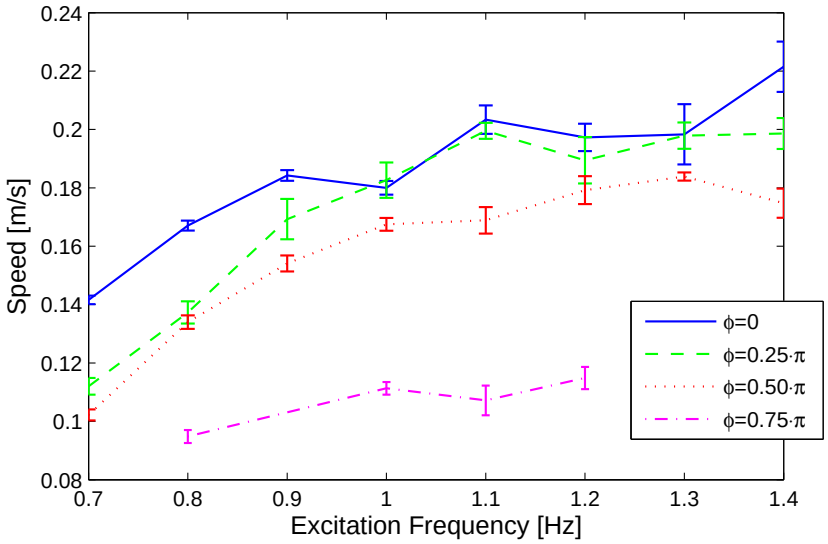

Figure 20: Speed vs. frequency for caudal fin 2 and the motorized body segment with different values of $\phi_{0,1}$

3.3.6 Speed of Pecotral Fins and all Fins

In this section we wanted on the one hand to analyze the speed using only pectoral fins as means of propulsion and then compare the superposition of the pectoral fin speed and the speed of the caudal fin and body segment to the actual speed of the robot propulsed by all its fin. We wanted to do this comparison because the movement of the robot induced by the horizontal movement of the caudal fin was quite different from the one one induced by the vertical movement of the pecotral fins and we wanted to know whether these two movements were linearly independent or whether they would influence each other in some way.

We used two pectoral fins with length $l = 0.05$ m, height $w = 0.04$ m, thickness $t = 0.003$ m and resonance frequency $f_{3R} = 2.6 \pm 1$ Hz. The excitation amplitude was at 80° for the pectoral fins (a smaller excitation amplitude had almost no effect on the speed), and 40° for the caudal fin and the motorized body segment respectively. Note that the movement of the pectoral fins was in phase, any offset between them resulted in a extrem drop of speed.

Figure 21 shows the result for the pectoral fins, the caudal fin and the motorized body segment (offset zero), the linear superposition of those two movements and the actual measured speed for the movement of all fins.

We can see that the pectoral and caudal fin movement are not linearly independent. We have to admit that the superposition we made is rather a simplification as the resistance of the water increases with the square of the speed, but still, the performance in terms of speed is even worse with the movement of the pectoral fins than without. This means that the two movements are actually interfering with each other. Maybe this is the reason that fish, at least the ones that have any physical ressemblance with our robot, do not use their pecotral fins for propulsion normally, but only for the smaller, more precise adjustements and in order to stay at the same point. It is possible that another configuration of the robot (cf. section 2.1) would allow two minimize these effects, although for the controller we used this is far from obvious.

Note that as the resonance frequency of the pectoral fins is very high we cannot observe any influence on the speed curve. Additionnally it is almost impossible to say which part of the movement of all the fins might more be due to the pectoral fins and which to the caudal fin.

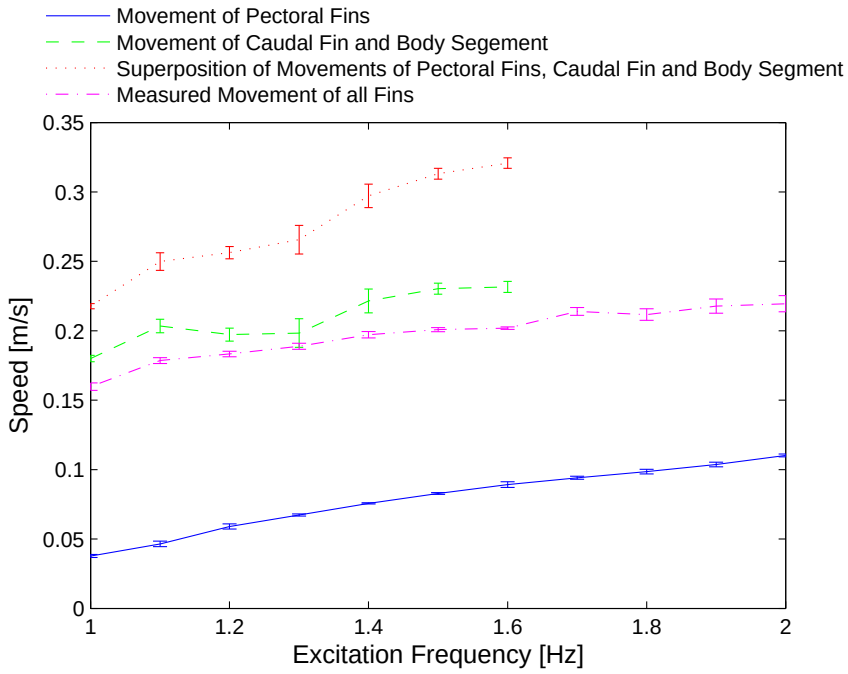

Figure 21: Movement of the pectoral fins and all fins together

3.3.7 Comparison with simulation

Figure 22 shows the difference between the measured and the simulated path of the robot over a swimming period of 10 seconds, propulsed by caudal fin 1 (95x40 mm) at $f = 1.0$ Hz and 60° excitation amplitude. Figure 23 shows the speed vs. frequency plot of that movement.

We can see immediately that the the simulated robot is much faster than the real one, which must be due to some problems with the hydromechanic parameters. Unfortunately we had no opportunity to optimize the hydromechanic coefficients in order to have similar results. Note that very certainly the real robot might at any rater be slower than the simulated one as there are many factors we do not take into account, for example turbulences due to wave reflection on the sides of the pool.

Note also that some influence of the resonance frequency might be guessed around 1.0 Hz, although only very faintly.

As the absolute value of the speed did not correspond to the real values, we finally decided only to refer to the relative change for our last measures.

Figure 24 shows the simulation of the speed for different values of the offset between caudal fin 2 and the motorized body segment.

We can see that the speed decreases for higher offset, which corresponds very well to the findings for the real robot (cf. section 3.3.5).

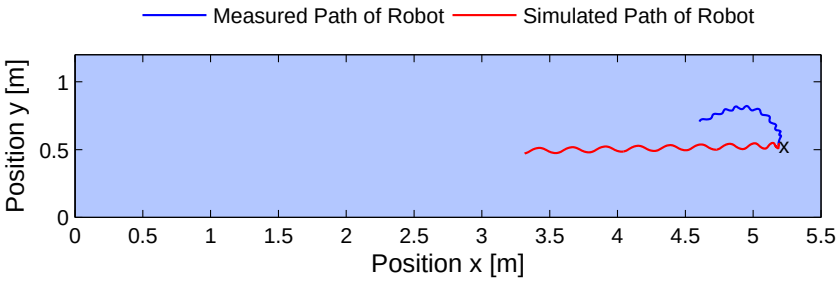

Figure 22: Measured and Simulated Path of the Robot starting at 'x' and swimming to the left for 10 seconds.

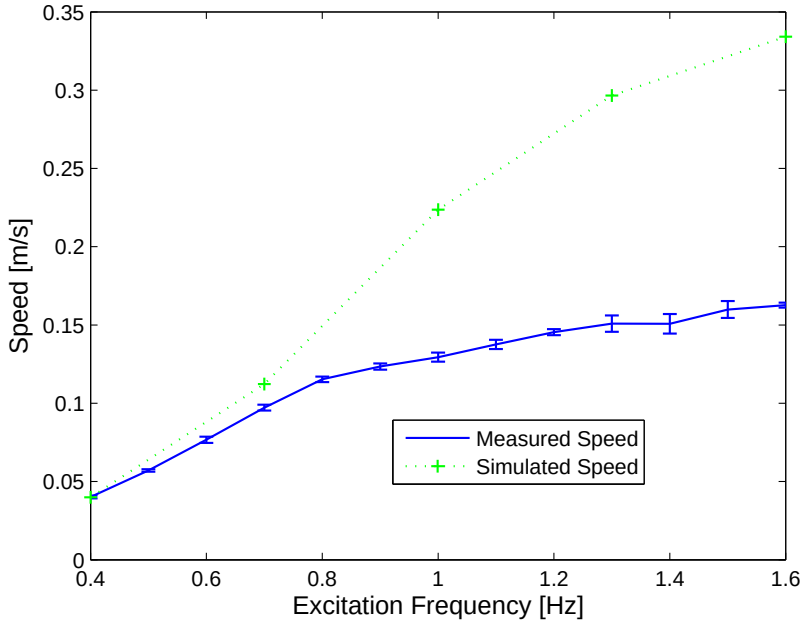

Figure 23: Measured and simulated speed vs. frequency for a robot propulsed by a caudal fin of 95x40 mm at $f = 1.0$ Hz and 60° excitation amplitude

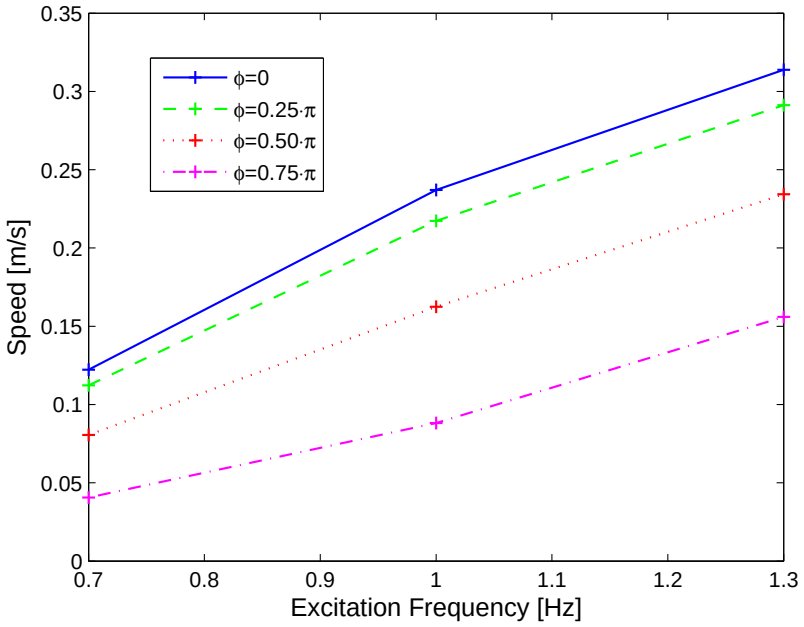

Figure 24: Simulated speed vs. frequency for caudal fin 2 and the motorized body segment with different values of $\phi_{0,1}$

3.4 Efficiency Estimation

A quick look at the Strouhal numbers depticted in figure 25 shows that optimality of vortex creation around the robot is quite far from the one of real fish, which are in a range of 0.2-0.4. However, we can see the large impact the resonance frequency has on the Strouhal number and thus the swimming efficiency of the robot. It can thus be seen that, in general, swimming at frequencies above the resonance frequency limit of the fins is not more efficient in some cases even less efficient.

This corresponds very well with our hypothesis and is a further proof of the fact that swimming at the resonance frequency is quite efficient. A efficient swim would thus be for a frequency slightly above the resonance frequency and an excitation amplitude around 60° using the pecotral fins only for diving and steering. Using a bigger fin in order to swim faster doesn't influence much the efficiency, whereas for not too big excitation amplitudes it seems to be worthwile to swim at higher frequencies.

Our findings for the Froude number, using equation 7 with $g = 10\,\frac{\mathrm{m}}{\mathrm{s}^2}$ and $L = 0.5$ m, show that $Fr_{max} = 0.09$. As this is much smaller than 1, we conclude that our robot has very low maneuverability.

We can also observe that the Reynold's number of our measures are above 10^6 even for very low speed and which means that the flow around our robot is turbulent.

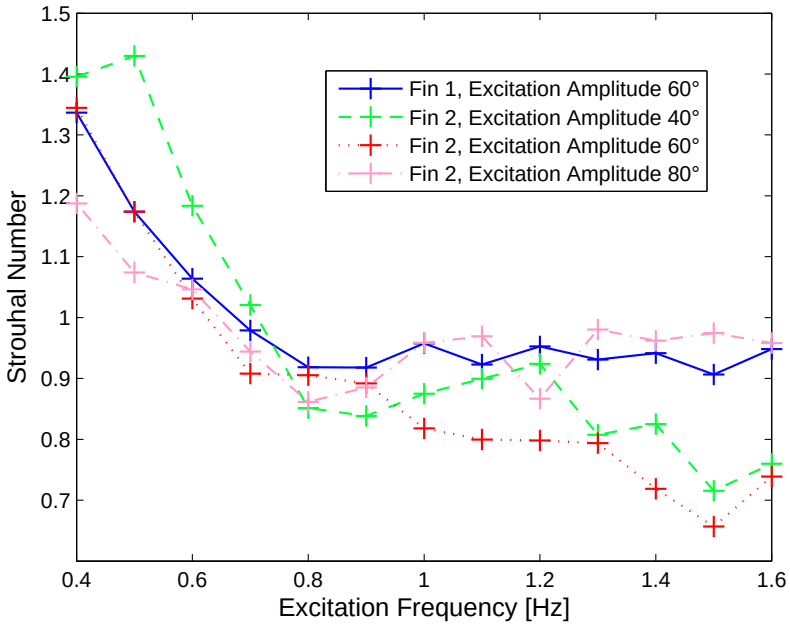

Figure 25: Strouhal numbers for different frequencies of the two caudal fins

4 Conclusion

This project dealt with the design and programmation of a more recent version of the BoxBot robot fish. The robot was tested in an real world environment and precise speed and position measures were taken in addition to the measures of fin amplitude and for several swimming frequencies.

We could show that the amplitude of a caudal fin was biggest around the resonance frequencym, that swimming at the resonance frequency was very efficient and that the speed of the robot could not be increased significantly for frequencies above this limit. We could see that a higher excitation amplitude resulted in higher speed, but that in terms of efficiency an excitation amplitude around 60° would perform best. We have also seen that the robot prefers carangiiform propulsion with a zero offset between its body segments and we could show that the speed of the robot is only slightly higher for a fin with bigger height.

Finally, we compared our results to values obtained by simulation and we could show that although the hydromechanic parameters surely need some optimization, the resonance curves obtained in simulaton show comparable results as the ones in a real world environment. From the simulation of the robot's speed one might guess that it is influenced by the resonance frequency and we saw that the simulated robot as the real one moved faster for a zero offset between its segments.

5 Further Work

As we could only take measures for two fins with comparable length it would be good to take fins of different size and see whether whether our hypothesisses still hold. One might also think of using different shapes of fins, maybe inspired by different fish families, for testing the speed and consider the influence of the fins aspect ratio. As we used only one material and always the same thickness of the fins, it could be interesting to take materials with different young's modulus, use fins that have a change in stiffness as this was shown to allow more efficient swimming [5].

As our measures so far have only shown that caudal and pectoral fin motion are completely interfering, we could try to analyze this effect into more detail and try to find better control and command methods.

One could do also measures of amplitude for the case of a movement of caudal fin and motorized body segment in order to predict its efficiency by means of the Strouhal numbers.

In another step one could also develop a better controller that would allow the robot to follow a given path very closely and not only a simple line as in our case. It would therefore be necessary to be able to detect the absolute position and orientation of the robot.

Once such a command and control system shows reliable results one could think of using evolutionary algorithms in order to do a characterization of the robot's swimming. This would allow to see whether artificial evolution would come up with comparable results as real evolution is was said to, for example short acceleration periods and longer gliding periods, in opposition to a steady propulsion we have implanted in our robot.

We might use different configurations of the robot together with a different kind of control and do some stablity measures.

Finally one could try to optimize the hydromechanic parameters and do more extended simulations in order to have a computational model that is as close to the real one as possible.

6 Acknowledgments

We are very grateful for all the support we have received from our close ones, but especially wanted to thank the people from the BIRG who would always be at hand with good and reliable practical and theoretical adivce. We wanted to thank in particular A. Crespi for all the occasions where he helped us solve impassable informatical problems, healed the robot whenever we thought it must have been completely broke and repaired the modules when we happend to do some short-curcuits and kill the electronics and we wanted to thank him for backing and assisting this semster project. We also wanted to thank M.Perez for his support concerning all the simulation and the modelling of the robot, his patience in explaining us very complex formulas and relating them to real world problems. Without the two of them, this project would not have been possible. We also wanted to thank A.Guignard for his support in the mechanical design of the robot. A big thank you goes finally, last but not least, to A.J.Ijspeert for giving this project his support, defining its major goals and making it possible for students to take part in very motivating and fullfilling projects with a strong link to true scientific research.

7 Bibliography

[1] D.Lachat: "BoxyBot, the fish robot: Design and Realization", BIRG, School of Computer and Communication Science, Ecole Polytechnique Fédérale de Lausanne (EPFL), Switzerland, 2005
[2] A.Pasquier: "BoxyBot, le robot poisson: Finition et présentation", BIRG, School of Computer and Communication Science, Ecole Polytechnique Fédérale de Lausanne (EPFL), Switzerland, 2006
[3] J.N.Newman: "Marine Hydrodynamics", MIT Press, 1977
[4] J.J.Rohr, F.E.Fish: "Strouhal numbers and optimization of swimming by odontocete cetaceans", *The Journal of Experimental Biology* 207, 1633-1642, 2004
[5] S.Heo, T.Wiguna, H.Ch.Park, N.S.Goo: "Effect of an Artificial Caudal Fin on the Performance of a Biomimetic Fish Robot Propelled by Piezoelectric Actuators", *Journal of Bionic Engineering* 4, 151−158, 2007
[6] A.Crespi, D.Lachat, A.Pasquier, A.J.Ijspeert: "Controlling swimming and crawling in a fish robot using a central pattern generator", BIRG, School of Computer and Communication Science, Ecole Polytechnique Fédérale de Lausanne (EPFL), Switzerland, 2005
[7] A. Crespi and A.J. Ijspeert. "AmphiBot II: An amphibious snake robot that crawls and swims using a central pattern generator", in: *Proceedings of the 9th International Conference on Climbing and Walking Robots (CLAWAR 2006)*, 2006.

Appendice

Calculating the Inertial Matrix The intertial matrix is given by:

$$\widehat{I_o} = \widehat{I_G} + m \cdot \widehat{\vec{OG}}^T \cdot \widehat{\vec{OG}}$$

where $\widehat{I_G}$ is the intertial matrix with respect to the center of gravity and $\widehat{\vec{OG}}$ is a matrix corresponding to $\vec{OG}$, the vector desribed in section 2.3.1 and given by:

$$\vec{OG} = \begin{pmatrix} x \\ y \\ z \end{pmatrix} = (\frac{l}{2} - e) \cdot \begin{pmatrix} 1 \\ 0 \\ 0 \end{pmatrix}$$

which corresponds to the fact that the inertial force is only attacking in the x direction. The module and its
The matrix $\widehat{\vec{OG}}$ is satisfying the general relation:

$$\vec{a} \times \vec{b} = \widehat{\vec{a}} \cdot b$$

It can thus be shown that:

$$\widehat{\vec{OG}} = \begin{pmatrix} 0 & -z & y \\ z & 0 & -x \\ -y & x & 0 \end{pmatrix} = (\frac{l}{2} - e) \cdot \begin{pmatrix} 0 & 0 & 0 \\ 0 & 0 & -1 \\ 0 & 1 & 0 \end{pmatrix}$$

The interial matrix $\widehat{I_G}$ is defined as follows:

$$\widehat{I_G} = \begin{pmatrix} I_{G,xx} & I_{G,xy} & I_{G,xz} \\ I_{G,yx} & I_{G,yy} & I_{G,yz} \\ I_{G,zx} & I_{G,zy} & I_{G,zz} \end{pmatrix}$$

which is a symetrical matrix.

In our case we can make the assumption that $I_{G,xy} = I_{G,xz} = I_{G,yz} = 0$ and as the matrix is symetrical we conclude that $\widehat{I_G}$ is a diagonal matrix, the elements of which are given by:

$$I_{G,xx} = \frac{m}{12} \cdot \left(h^2 + w^2\right)$$

$$I_{G,yy} = \frac{m}{12} \cdot \left(l^2 + h^2\right)$$

$$I_{G,zz} = \frac{m}{12} \cdot \left(l^2 + w^2\right)$$

We can therefore write:

$$\widehat{I_O} = \begin{pmatrix} I_{O,xx} & I_{O,xy} & I_{O,xz} \\ I_{O,yx} & I_{O,yy} & I_{O,yz} \\ I_{O,zx} & I_{O,zy} & I_{O,zz} \end{pmatrix}$$

with

$$I_{O,xx} = \frac{m}{12} \cdot \left(h^2 + w^2\right)$$

$$I_{O,yy} = \frac{m}{12} \cdot \left(l^2 + h^2\right) + m \cdot (\frac{l}{2} - e)^2$$

$$I_{O,zz} = \frac{m}{12} \cdot \left(l^2 + w^2\right) + m \cdot (\frac{l}{2} - e)^2$$

and $I_{O,xy} = I_{O,xz} = I_{O,yz} = 0$. And as the matrix is also symetrical we are again dealing with a diagonal matrix.

Calculating the Thrust Force Suppose a reference frame fixed to the head of the robot and given by the vectors $\vec{e_1}, \vec{e_2}, \vec{e_3}$ as well as a reference frame fixed to the trailing edge of the caudal fin and given by the vector $\vec{t_1}, \vec{t_2}, \vec{t_3}$. Let's further suppose that $\vec{t_1}$ is always tangent to the caudal fin. The thrust force is then given by:

$$F_t = (-\frac{1}{2} \cdot m_f \cdot |\vec{v_2}|^2 \cdot \vec{t_1} + \vec{v_1} \cdot \vec{v_2} \cdot m_f \cdot \vec{t_2}) \cdot e_1$$

where $\vec{v_1} = |\vec{v_c}| \cdot \vec{t_1}$ and $\vec{v_2} = |\vec{v_c}| \cdot \vec{t_2}$, $\vec{v_c} = (v_x, v_y, v_z)^T$ is the speed vector and m_f the added mass, given in this case by $m_f = \rho_f \cdot \pi \cdot \left(\frac{h}{2}\right)^2$. h is of course the height of the fin and ρ_f is the density of the fluid.

The speed vectors gives the speed of the caudal fin at the trailing edge and can be calculated by summing up all the different speeds ω_i of every interconnection obtained by the simulator. To do this we used the following recurrent formulas:

$$\vec{\Omega_j} = \vec{\Omega_{j-1}} + \omega_i \cdot \vec{e_3}$$

$$\vec{V_j} = \vec{V_{j-1}} + \vec{\Omega_j} \times \vec{d_j}$$

where $\vec{d_j}$ is the vector which gives the distance between two interconnections in the reference frame given by the vectors $\vec{e_1}, \vec{e_2}, \vec{e_3}$.

Using the initial values of $\vec{\Omega_0} = 0$ and $\vec{V_0} = 0$, we obtain the speed vector for a system with n interconnections by $\vec{v_c} = \vec{V_n}$.

The vectors of the reference frame fixed to the trailing edge can be obtained in a similar way, summing up all the different angles ϕ_i, thus calculating the reference frame for every segment until we arrive at the trailing edge.

Error Calculation for the young's modulus Using equation 5, we can easily see that the young's modulus is given by:

$$E(f) = \frac{4\pi^2 \cdot f^2 \cdot l^4}{t^3} \cdot (4\rho_f \cdot t + \pi\rho_w \cdot w)$$

It can then be seen that, according to error theory and using a first order taylor series as approximation, the error on the young's modulus is given by:

$$\Delta E(f) = \frac{dE(f)}{df} \cdot \Delta f = \frac{8\pi^2 \cdot f \cdot l^4}{t^3} \cdot (4\rho_f \cdot t + \pi\rho_w \cdot w) \cdot \Delta f$$